

Development of a Collisional Radiative Model for Hydrogen-Caesium Plasmas and its Application to the Measurement of Caesium Density in SPIDER

B. Pouradier Duteil, E. Sartori, B. Zaniol, M. Barbisan, C. Poggi and G. Serianni

Abstract—SPIDER (Source for the Production of Ions of Deuterium Extracted from a Radio frequency plasma) is the full scale prototype for the ITER Heating Neutral Beam (HNB) source. The production of negative ions in the source mostly relies on the conversion of H/D atoms and positive ions on a converter surface, which is covered with caesium in order to reduce its work function and maximise the conversion efficiency. Caesium is transported to the converter during both the vacuum and the plasma phases, and caesium coverage should be properly balanced. Therefore, the study of caesium density and transport in the source plays a crucial part in understanding and monitoring the ion production.

During plasma operation, the measurement of caesium density and population distribution in the source can be obtained by Optical Emission Spectroscopy (OES). This is done by tracking the intensity of certain caesium emission lines and comparing these measurements with models mimicking the dynamics of caesium in the plasma. A collisional radiative (CR) model for low temperature hydrogen-caesium plasmas was recently developed in order to perform such measurements in SPIDER. It includes the caesium ground-state and 14 excited states evolving in a background made up of singly charged caesium positive ions, electrons, hydrogen atoms and negative ions. If enough emission lines are detected, the model can be used to characterize the Cs density in the source thanks to the many lines-of-sight available. On the other hand, if few lines are detected, the model can be combined with direct measurements of the caesium density made by Laser Absorption Spectroscopy (LAS) to provide estimates of the plasma parameters. This work describes the model and its use in conjunction with OES during the first operation with caesium in SPIDER.

I. INTRODUCTION

IN order to meet the thermonuclear-relevant plasma parameters of ITER, an efficient operation of the Heating Neutral Beam injectors (HNB) is required. ITER will be provided with two HNBs, designed to inject beams of deuterium atoms accelerated at a maximum of 1 MeV, delivering a power of 16.5 MW during pulses of up to 3600s [1]. The Neutral Beam Test Facility (NBTF), hosted in Padova, Italy, includes two experiments: MITICA, the full-scale prototype of the ITER HNB, and SPIDER, the full-size radio-frequency (RF)

negative-ion source that is already in operation [2].

In SPIDER, the plasma is produced by 8 cylindrical drivers powered in pairs by 4 RF oscillators, each reaching powers up to 200 kW with a driving frequency of 1 MHz. The drivers are connected to an expansion chamber, at the end of which the beam is extracted and accelerated to energies up to 110 keV by a set of three grids, starting with the Plasma Grid (PG) facing the plasma. A Bias Plate (BP) is mounted 10 mm upstream of the PG and is used to optimize the electric field in the region near the PG (where most of the negative ion generation occurs) by varying its potential.

The volume-production yield of negative ions in the source is insufficient to meet the requirements for SPIDER, this can only be done by taking advantage of surface-production, i.e. charge exchange of positive ions or atoms with a converter surface. The efficiency of this negative-ion generation process exponentially increases with the decrease of the surface's work function, which describes the energy needed to remove an electron from a solid. The work function of the surfaces facing the plasma, and in particular the PG, is minimized by coating them with caesium (the metal with the lowest work function of all) by evaporating it into the source [3]. Three Cs ovens are located at SPIDER's back-plate, and enable a uniform evaporation in the source with a precise control of the evaporation rate [4]. In the case of a pure layer of Cs on the converter surface, the minimum work function is obtained for a thickness of less than a monolayer, and a more uniform distribution of Cs is obtained by combining the effects of the plasma and of the heating of the surfaces. The study of Cs density and transport in the source plays an essential part in monitoring the negative-ion production.

During plasma operation, the measurement of caesium density and population distribution in the source can be obtained through Optical Emission Spectroscopy (OES) [5], [6]. The intensity of the emission lines resulting from the de-excitation of Cs atoms are tracked and the caesium ground state density is calculated with the help of models mimicking the behavior of Cs in low temperature caesium-hydrogen plasmas. Creating

This work has been carried out within the framework of the ITER-RFX Neutral Beam Testing Facility (NBTF) Agreement and has received funding from the ITER Organization. The views and opinions expressed herein do not necessarily reflect those of the ITER Organization. This work has also been carried out within the framework of the EUROfusion Consortium and has received funding from the Euratom research and training programme 2014-2018 and 2019-2020 under grant agreement No 633053. The views and opinions expressed herein do not necessarily reflect those of the European Commission. This work was supported in part by the Swiss National Science Foundation. (Corresponding author: B. Pouradier Duteil)

B. Pouradier Duteil is with the Ecole Polytechnique Fédérale de Lausanne (EPFL), Swiss Plasma Center (SPC), CH-1015 Lausanne, Switzerland, seconded to Consorzio RFX, Corso Stati Uniti 4, I-35127, Padova, Italy (e-mail: basile.pouradierduteil@epfl.ch)

E. Sartori is with Consorzio RFX, Corso Stati Uniti 4, I-35127, Padova, Italy and also with the Università degli Studi di Padova, Strad. S. Nicola 3, I-36100 Vicenza, Italy

B. Zaniol, M. Barbisan, C. Poggi and G. Serianni are with Consorzio RFX, Corso Stati Uniti 4, I-35127, Padova, Italy

such a model was motivated by the following reasons:

- SPIDER is equipped with a great number of lines-of-sight (LoSs). Using emission spectroscopy to monitor the Cs density can provide a spatial resolution that other diagnostics cannot produce.
- It is well known that the ratio between vacuum phase and plasma phase durations (the duty cycle) strongly affects Cs transport in the source [7]. The interpreted Cs density distribution can help clarify the role of discontinuous plasma discharges in creating an optimal Cs layer at the PG.
- The distribution of caesium in the source can be compared with the negative-ion beamlet currents to determine the effect of the uniformity of caesium at the PG on the uniformity of extracted currents.
- Given enough Cs emission lines, or given values of the Cs density from another diagnostic, plasma parameters can be estimated

A collisional radiative (CR) model was developed and its results compared with existing models found in the literature. When the results of the model were deemed satisfactory, a large number of simulations was performed to cover a wide range of plasma parameters. A set of scripts was written to carry out the interpretation of the Cs lines in quasi real time during operation in SPIDER.

II. DEVELOPMENT OF THE CR MODEL

Two CR models dedicated to caesium and its detection in large negative ion sources for Neutral Beam Injectors are described in the literature. The work by Wunderlich et al. [8] addresses the main ingredients of a Cs-H CR model, which is successfully applied to Neutral Injector (NI) prototype sources. The work by Priti et al. [9] reports a full list of cross-sections for Cs excitation by electron impact, fine-structure resolved, with their fitting parameters. Additionally, cross sections for caesium-hydrogen interactions are reported by Belyaev et al. [10].

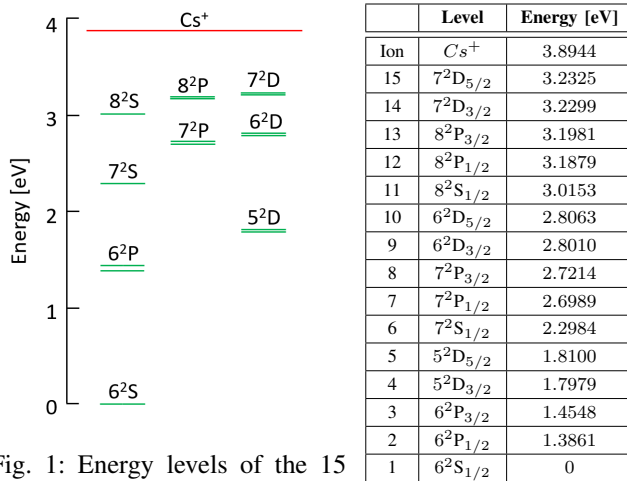


Fig. 1: Energy levels of the 15 Cs⁰ states of the model

The CR model was implemented starting from those works and the cross-sections reported by these authors (Table I), and

studies the distribution of the Cs ground state and of the first 14 excited states (Fig. 1). The excited states with higher energies are not included because of the lack of precise cross-sections for the excitation and de-excitation processes of these levels in the literature.

TABLE I: Reactions included in the model (state $i < j$)

Process	Reaction	Ref.
Spontaneous emission	$Cs^{0,j} \rightarrow Cs^{0,i} + \gamma$	[9]
e ⁻ collision excit.	$Cs^{0,i} + e^- \rightarrow Cs^{0,j} + e^-$	[9]
e ⁻ collision de-excit.	$Cs^{0,j} + e^- \rightarrow Cs^{0,i} + e^-$	Det. balance
H collision excit.	$Cs^{0,i} + H \rightarrow Cs^{0,j} + H$	[10]
H collision de-excit.	$Cs^{0,j} + H \rightarrow Cs^{0,i} + H$	[10]
Ionisation	$Cs^{0,i} + e^- \rightarrow Cs^+, e^-, e^-$	[9]
3-body recombination	$Cs^+, e^-, e^- \rightarrow Cs^{0,i} + e^-$	[8]
Radiative recombination	$Cs^+, e^- \rightarrow Cs^{0,i} + \gamma$	[8]
Mutual neutralization	$Cs^+, H^- \rightarrow Cs^{0,i} + H$	[8]

Given a set of plasma parameters (T_e , n_e , n_{H^0} , n_{H^-} , etc.) the Cs⁰ populations evolve according to the different excitation and de-excitation processes. The steady state of the population distribution is resolved through an iterative scheme. T_e , n_e and n_{H^-} scans were performed and compared with identical simulations carried out by Wunderlich et al. and Priti et al. Figures 2, 3 and 4 feature the dependence of 3 populations (6 taking into account the fine structure) on the three plasma parameters. The decision to examine these three populations comes from the fact that their de-excitation wavelengths are observable by emission spectroscopy (400-900 nm) and at emission frequencies large enough to expect the lines to appear above the spectrum noise (Table II).

TABLE II: Main de-excitation channels observable with OES

Upper level	Lower level	Emission freq. [s ⁻¹]	λ [nm]
7 ² P _{3/2}	6 ² S _{1/2}	$1.93 \cdot 10^6$	455.7
7 ² P _{1/2}	6 ² S _{1/2}	$7.45 \cdot 10^5$	459.4
7 ² D _{3/2}	6 ² P _{1/2}	$6.45 \cdot 10^6$	672.5
7 ² D _{5/2}	6 ² P _{3/2}	$7.15 \cdot 10^6$	697.5
7 ² D _{3/2}	6 ² P _{3/2}	$1.22 \cdot 10^6$	698.5
8 ² S _{1/2}	6 ² P _{3/2}	$4.58 \cdot 10^6$	794.6
6 ² P _{3/2}	6 ² S _{1/2}	$3.33 \cdot 10^7$	852.3
6 ² D _{3/2}	6 ² P _{1/2}	$1.09 \cdot 10^7$	876.4
8 ² P _{3/2}	5 ² D _{3/2}	$3.90 \cdot 10^4$	885.6
8 ² P _{1/2}	5 ² D _{3/2}	$4.34 \cdot 10^5$	892.1
8 ² P _{3/2}	5 ² D _{5/2}	$2.77 \cdot 10^5$	893.3
6 ² P _{1/2}	6 ² S _{1/2}	$3.03 \cdot 10^7$	894.6

The population distribution highly depends on the electron density and temperature, and the model provides results similar to those of the models discussed in [8] and [9]. However, some discrepancies can be noticed, especially for the 7²D population. As shown in Table I, the reaction probabilities of the processes included in the model do not come from a single source, the set of cross-sections is therefore not identical to the one used in [8] or in [9], and slight differences in the results produced by the three models can be expected. Figure 4 shows the importance of including the mutual neutralization of Cs⁺

and H^- in the model for $n_{H^-} > 10^{16} \text{ m}^{-3}$. However, these simulations were performed with $n_{Cs^+}/n_{Cs^0} = 9$: section III-A describes how such a ratio might not be suitable in the case of SPIDER at the specific lines-of-sight considered in this paper. Reducing the ratio to a value of 0.5-1 would make the mutual neutralization processes less relevant for H^- densities lower than n_e .

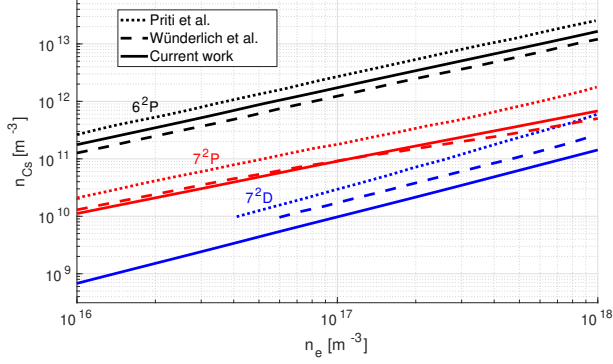


Fig. 2: Cs population distribution dependence on n_e ($n_{Cs} = 10^{15} \text{ m}^{-3}$, $T_e = 2 \text{ eV}$, $n_{H^-} = 0$, $n_{H^0} = 10^{19} \text{ m}^{-3}$, $n_{Cs^+}/n_{Cs^0} = 9$)

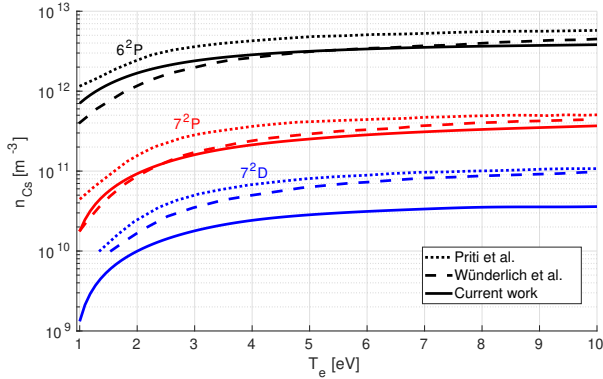


Fig. 3: Cs population distribution dependence on T_e ($n_{Cs} = 10^{15} \text{ m}^{-3}$, $n_e = 10^{17} \text{ m}^{-3}$, $n_{H^-} = 0$, $n_{H^0} = 10^{19} \text{ m}^{-3}$, $n_{Cs^+}/n_{Cs^0} = 9$)

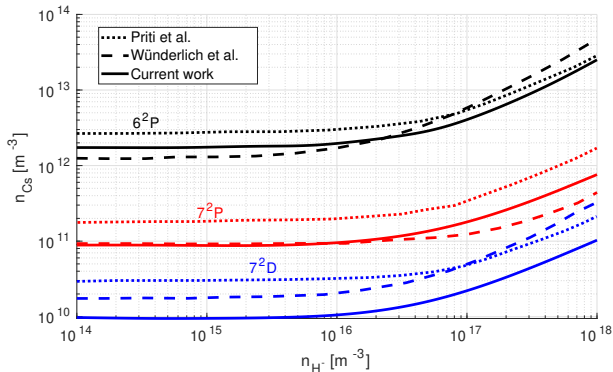


Fig. 4: Cs population distribution dependence on n_{H^-} ($n_{Cs} = 10^{15} \text{ m}^{-3}$, $n_e = 10^{17} \text{ m}^{-3}$, $T_e = 2 \text{ eV}$, $n_{H^0} = 10^{19} \text{ m}^{-3}$, $n_{Cs^+}/n_{Cs^0} = 9$)

III. USE OF THE MODEL IN SPIDER

Figure 5 shows the lines-of-sight used during SPIDER's first operation with Cs. The LoSs are all horizontal and parallel to the PG. The OES LoSs are located at 5 mm (red), 17 mm (light green), 35 mm (yellow) and 67 mm (magenta) from the PG, the LAS LoSs (blue squares) are at 25 mm from the PG.

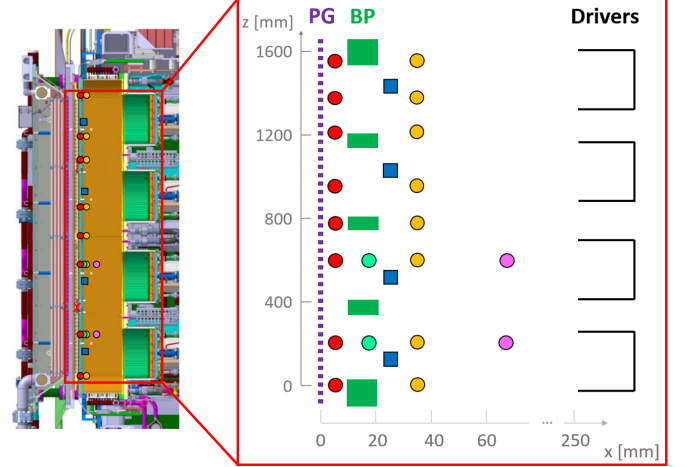


Fig. 5: Positions of the OES LoSs (red, green, yellow & magenta) and LAS LoSs (blue) in SPIDER (vertical section)

A. Discussion on the $\frac{Cs^+}{Cs^0}$ ratio at the PG

The simulations displayed on figures 2, 3 and 4 were performed with the Cs ion-to-atom ratio fixed at a value of 9 in order to use parameters comparable with the results presented in [8] and [9]. However, fixing the ratio to this value is an assumption that might not always be valid in the case of SPIDER: it strongly depends on the plasma parameters and on the vicinity to surfaces in the source.

Cs^+ ions impinging on a surface are neutralized and reflected back into the plasma, resulting in a net flux of Cs^0 that therefore depends on the local density of Cs^+ . The flux of Cs^0 coming from the PG and BP must be taken into account as the low electron density and temperature make for a Cs ionization mean free path of the order of $\sim 10 \text{ cm}$: a large part of the Cs^0 exiting the surfaces is not yet ionized at these distances.

Adding this element of transport to the system, the balance equation of the density of Cs atoms becomes:

$$0 = (\Gamma_{in} - \Gamma_{out}) \cdot A + \left(X_{rad. rec.} n_e n_{Cs^+} + X_{3 body rec.} n_e^2 n_{Cs^+} + X_{mut. neutr.} n_{H^-} n_{Cs^+} - X_{ioniz.} n_e n_{Cs^0} \right) \cdot Al \quad (1)$$

where

- $X_{rad. rec.}$ [$\text{m}^3 \text{s}^{-1}$], $X_{3 body rec.}$ [$\text{m}^6 \text{s}^{-1}$] and $X_{mut. neutr.}$ [$\text{m}^3 \text{s}^{-1}$] are respectively the radiative recombination, 3-body recombination and mutual neutralization (with H^-) reaction rates
- X_{ioniz} [$\text{m}^3 \text{s}^{-1}$] is the ionization rate
- A [m^2] is the area facing the PG and l [m] the width of the volume considered ($V = A \cdot l$)

- Γ_{in} and Γ_{out} are the fluxes of Cs^0 desorbed from the surfaces entering and exiting the volume.

This problem is uni-dimensional, as the area A can be eliminated. The flux of Cs^0 exiting a surface ($\Gamma_{\text{Cs}^0, \text{Surface} \rightarrow \text{Plasma}}$ or $\Gamma_{\text{Cs}^0, S \rightarrow P}$) is estimated as

$$\begin{aligned}\Gamma_{\text{Cs}^0, S \rightarrow P} &= \Gamma_{\text{Cs}^+, P \rightarrow S} = v_{\text{Cs}^+} \cdot n_{\text{Cs}^+} \\ &= \frac{1}{2} n_{\text{Cs}^+} (d_{\text{surface}} = 0) \sqrt{\frac{kT_e}{m_{\text{Cs}}}}\end{aligned}\quad (2)$$

This assumption comes from the fact that, in the case where the surface is covered with a sufficient layer of Cs, the exiting particles are either due to Cs^0 particles reflected on the surface (in which case the net flux of Cs^0 is 0) or to Cs^+ particles being neutralized and reflected after impinging on the surface. The velocity of the Cs^+ arriving at the surface is given by the Bohm velocity of the plasma sheath. Equations (1) and (2) are combined to estimate the flux of Cs^0 exiting the surface and the corresponding Cs ion-to-atom ratio at the lines-of-sight closest to the PG. Once this flux is known, equation (1) can be used to determine the ion-to-atom ratio at distances further away from the surface by using

$$\Gamma_{in} - \Gamma_{out} = \Gamma_{\text{Cs}^0, S \rightarrow P} \cdot \left(e^{-\frac{x-l/2}{\lambda_{ion}}} - e^{-\frac{x+l/2}{\lambda_{ion}}} \right)$$

where x [m] is the distance from the PG and λ_{ion} [m] is the Cs atom ionization mean-free-path.

Figure 6 shows the results of such an estimation. The profiles chosen for n_e and T_e are the results of electrostatic probe measurements made in SPIDER during a previous experimental campaign. The negative ion profile is given by $n_{H^-} = 5 \cdot 10^{16} e^{-x/\lambda_C}$, where $\lambda_C = 0.375$ m is the combined mean-free-path of the hydrogen negative ion in a caesiated ion source, as calculated by Bacal et al. [11] for plasma parameters similar to those considered here.

These assumptions are far from being a complete description of the system, as they lack a proper description of the fluxes of Cs atoms and ions coming from different parts of the source (e.g. the contribution of fluxes resulting from sputtering at the backplate are neglected given the limited number of beam apertures used during the experimental campaign discussed in this work). The computed Cs ion-to-atom ratio is very sensitive to changes in n_e and n_{H^-} , these estimates must be considered cautiously. However, they do provide some indication on the expected order of magnitude of $\frac{n_{\text{Cs}^+}}{n_{\text{Cs}^0}}$, which will be set at 0.5 in all of the results shown in section IV.

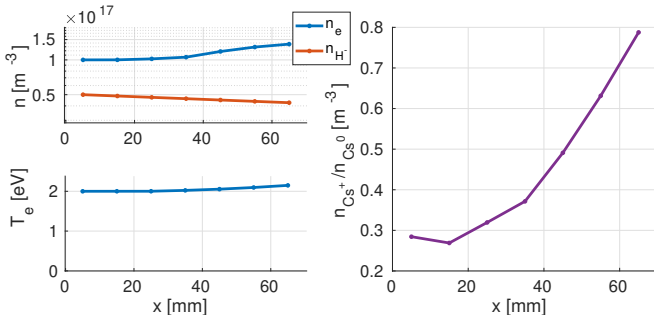


Fig. 6: Estimation of the Cs ion-to-atom ratio as a function of the distance to the PG

B. Method for the measurements in SPIDER

In SPIDER, optical emissions from the plasma are collected along various lines-of-sight. A number of peaks appear at the different wavelengths of the photons emitted by de-excitation of the Cs atoms (provided that the corresponding emitting population and emission frequency are large), these peaks are then integrated to provide a photon flux for this particular de-excitation. The photon flux at a specific wavelength λ can be related to the emitting population density by integrating the photon emission along the line of sight:

$$\Gamma_\lambda = \int_L n_{\text{Cs}^0, i}(l) \cdot f dl$$

where Γ_λ [$\text{m}^{-2}\text{s}^{-1}$] is the photon flux of a specific de-excitation channel, $n_{\text{Cs}^0, i}$ [m^{-3}] the volume density of the emitting Cs level i , f [s^{-1}] the de-excitation frequency and L [m] the length of the emitting plasma seen by the apparatus. Assuming that the excited population's density is uniform along the line of sight, it can then be estimated as:

$$n_{\text{Cs}^0, i} = \frac{\Gamma_\lambda}{f \cdot L}$$

The OES measurements used in conjunction with the CR model can be used in two ways to provide different types of information:

- Provided that enough Cs emission lines can be measured, the CR model can be used to find the ground-state density and estimate the plasma parameters
- On the other hand, if we are provided with a measurement of the Cs ground state density from another diagnostic such as LAS, the model can be used to estimate plasma parameters

IV. EXPERIMENTAL RESULTS

A. Experimental method

The results discussed in this section were derived from a single Cs emission line (at 852 nm, corresponding to the $6^2\text{P}_{3/2} \rightarrow 6^2\text{S}_{1/2}$ emission channel). The low electron temperature (2-3 eV) in the region near the BP and PG implies that the excited states of Cs are poorly populated and the emission lines are therefore difficult to distinguish from the spectrum noise or covered by hydrogen emissions. Other emission lines were identified, but their processing requires a more intricate procedure that is still ongoing and are therefore not considered here. As a consequence, the model cannot be used to estimate the Cs density on its own.

However, some information can still be derived from the intensity of this unique emission line if some hypotheses are made and provided as inputs to the model. A number of LoSs used for OES are located near a set of LoSs used for Laser Absorption Spectroscopy (LAS), a diagnostic enabling a direct measure of the Cs ground-state density [12]. Using these Cs density measurements as inputs, the model and OES measurements can be used as a tool to estimate the plasma parameters.

The results presented in sections IV-B and IV-C make use of OES measurements taken during three plasma pulses for

which the source operating parameters were identical, except for the Cs ovens' total evaporation rate (6, 12 or 24 mg/h). The main machine parameters were : power of the driver oscillators $P = 4 \times 100$ kW, filling pressure $p = 0.4$ Pa, Plasma Grid filter field current $I_{PG} = 1.5$ kA, Bias Plate and source bias currents $I_{ISBP} = I_{ISBI} = 80$ A.

B. Vertical profiles

Figure 7 features vertical profiles made during the three pulses at 35 mm from the PG. The LAS n_{Cs} measurements of fig. 7b demonstrate a clear correlation between the ovens' evaporation rate and the Cs density in the source, as expected. It reaches a maximum at mid-height, which can be explained by the fact that this is where the regions covered by the three Cs ovens overlap. Furthermore, the Cs density appears to be larger in the upper region than in the lower region. This could be due to a combination of the slight differences in behavior between the three ovens and of the redistribution mechanisms of the Cs in the source during the plasma phases. The electron density estimations featured on figure 7c are the result of combining the OES measurements with assumptions on

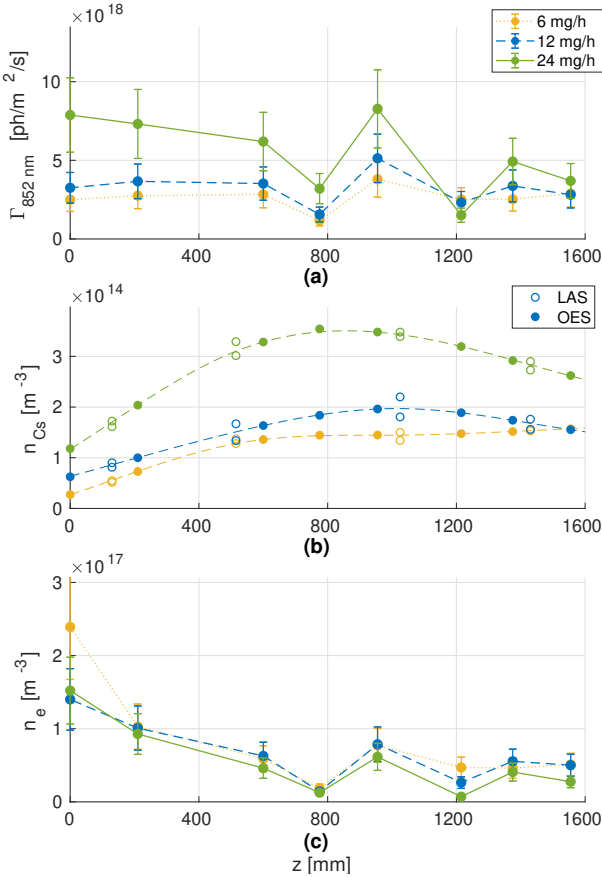


Fig. 7: Vertical profiles at 35 mm from the PG of (a) 852 nm emission line photon flux (b) n_{Cs} used as input for the model (extrapolated from the LAS measurements), (c) n_e as output of the model.

$T_e = 2.5$ eV, $n_{H-} = 4 \cdot 10^{16}$, $5 \cdot 10^{16}$, $7 \cdot 10^{16} \text{ m}^{-3}$ for the cases 6, 12, 24 mg/h respectively

n_{Cs} (fig. 7b) and on T_e . The assumptions on the Cs density are extrapolations of the LAS measurements, while the electron temperature is chosen to be $T_e = 2.5$ eV. The numbers chosen for n_{H-} are taken from measurements made by Cavity Ring Down Spectroscopy (CRDS) [13] at 5 mm from the PG and at the vertical position $z \approx 400$ mm.

The overall trend shows a higher electron density in the bottom of the source with respect to the upper part. The lower values at the ~ 800 mm and ~ 1200 mm marks owe to the positions of the LoSs in the source : these two LoSs, unlike the six other, are not located directly in front of a driver and therefore see a slightly weaker plasma. Similar vertical profiles are performed at 5 mm from the PG, assuming that the Cs density at this location is equal to what is measured by the LAS at 25 mm from the PG. The validity of this assumption is however unlikely for 4 of the 8 LoSs available at this distance, since those at $z \approx 0, 800, 1200$ and 1600 mm are located between the PG and the structure of the BP (fig. 5) implying that the plasma parameters and Cs transport conditions are very different from the regions that are not shaded by the BP. The error bars reported on the estimates of n_e are the results of the uncertainty of the measurements of Γ_{852nm} (estimated at $\pm 30\%$, mostly due to the oscillations of the spectrometer transfer function in the 800-900 nm region).

The PG and BP are equipped with electrostatic probes embedded in the side facing the drivers [14]. The ion saturation current measured by these probes is used to derive estimates of the density of the positive species in the plasma : assuming quasi-neutrality (ie. $n_+ \approx n_e + n_{H-}$), the hydrogen negative-ion density can thus be estimated.

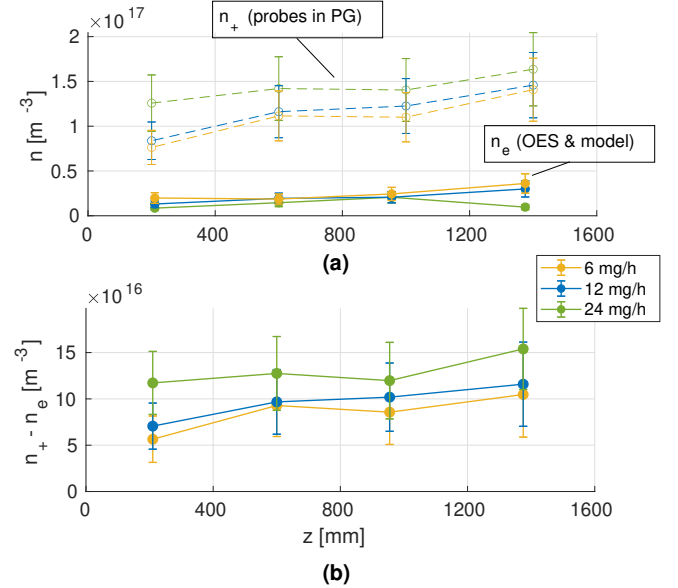


Fig. 8: (a) n_+ measured with the electrostatic probes in the PG and n_e (at 5 mm from the PG) from OES & CR model (b) Ensuing $n_{H-} \approx n_+ - n_e$ $T_e = 2$ eV, $n_{H-} = 5 \cdot 10^{16}$, $6 \cdot 10^{16}$, $8 \cdot 10^{16} \text{ m}^{-3}$ for the cases 6, 12, 24 mg/h respectively

Figure 8b shows the results of such an estimation at 5 mm from the PG. The ion density computed with this method is

higher than what is measured by CRDS by a factor of ~ 1.5 , which could be explained by the fact that the LoS used by CRDS is downstream of a segment of the BP, where the Cs coverage might not be optimal. Increasing the evaporation rate of the Cs ovens leads to a strong increase of the H^- density near the PG, and also seems to improve the vertical uniformity of n_{H^-} . Both of these effects impact the beam performance and are consistent with observations made by beam diagnostics during the same pulses. [15]

C. Horizontal profiles

In addition to the vertical profiles shown in the previous section, the large number of lines-of-sight available for OES measurements grant the possibility of performing horizontal profiles at certain vertical positions. Figure 9a shows the 852 nm line intensity as a function of the distance from the PG, at the vertical position $z = 600$ mm.

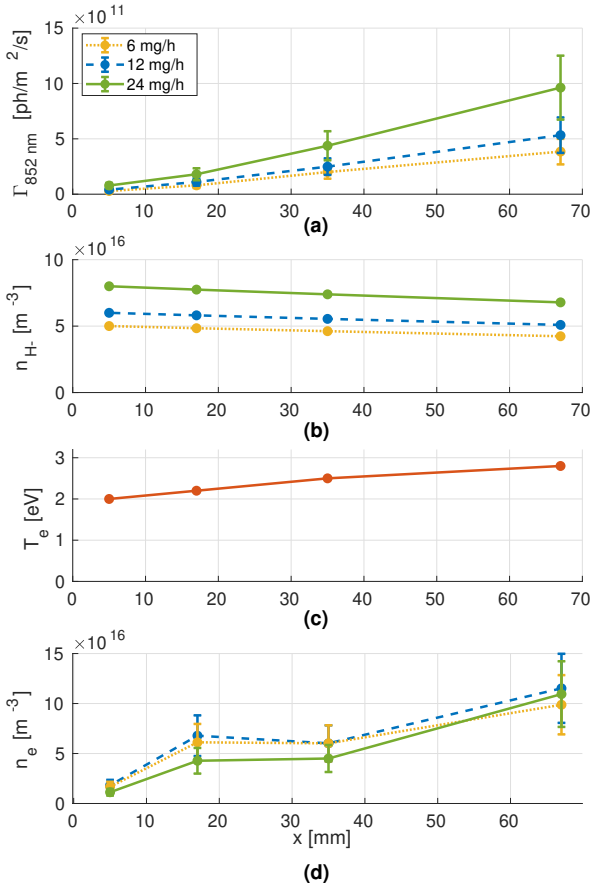


Fig. 9: Horizontal profiles (at $z \approx 600$ mm) of (a) 852 nm line OES intensity, (b) hypotheses on n_{H^-} , (c) hypotheses on T_e , (d) n_e as output of the model

The Cs density is assumed to be constant along the x-axis. On the other hand, the electron temperature is expected to increase as we draw closer to the drivers. Measurements made with movable electrostatic probes during a previous experimental campaign (prior to operations with Cs) are used to construct a T_e axial profile. As expected, the electron density output by the model rises substantially as the LoSs get closer to the drivers,

and increasing the Cs evaporation rate to 24 mg/h seems to reduce the amounts of electrons in the first cm near the PG.

V. CONCLUSION

A collisional radiative model for low-temperature and low-pressure Cs-H plasmas was developed. It was compared with data from pre-existing models discussed in the literature, and the results were found to agree well.

Considerations about the ion-to-atom ratio were made, and suggested that the ratio can fall to values of the order of 0.5 when approaching the PG.

OES measurements were performed and using Cs density measurements made with LAS, vertical and axial profiles of the electron density were carried out and provided interesting results consistent with the behavior of the beam.

A more comprehensive study of the Cs transport in the source should be completed and integrated to the model. With measurements of additional emission lines, the model and OES can be used as a tool to measure the electron density, temperature and Cs density, thus joining the multitude of diagnostics used to monitor Cs transport and negative-ion production in the source.

REFERENCES

- [1] V. Toigo *et al.*, "The PRIMA test facility: SPIDER and MITICA test-beds for ITER neutral beam injectors," *New Journal of Physics*, vol. 19, p. 085004, aug 2017.
- [2] V. Toigo *et al.*, "On the road to ITER NBIs: SPIDER improvement after first operation and MITICA construction progress," *Fusion Engineering and Design*, vol. 168, p. 112622, 2021.
- [3] Y. Belchenko *et al.*, "A powerful injector of neutrals with a surface-plasma source of negative ions," *Nuclear Fusion*, vol. 14, pp. 113–114, 1974.
- [4] M. De Muri *et al.*, "SPIDER Cs ovens functional tests," *Fusion Engineering and Design*, vol. 167, p. 112331, 2021.
- [5] B. Zaniol *et al.*, "First measurements of optical emission spectroscopy on SPIDER negative ion source," *Review of Scientific Instruments*, vol. 91, p. 013103, 2020.
- [6] U. Fantz *et al.*, "Diagnostics of the cesium amount in an rf negative ion source and the correlation with the extracted current density," *Fusion Engineering and Design*, vol. 74, pp. 299–303, 2005, proceedings of the 23rd Symposium of Fusion Technology.
- [7] A. Mimo *et al.*, "Modelling of caesium dynamics in the negative ion sources at BATMAN and ELISE," *AIP Conference Proceedings*, vol. 1869, p. 030019, 2017.
- [8] D. Wünderlich *et al.*, "A collisional radiative model for low-pressure hydrogen-caesium plasmas and its application to an rf source for negative hydrogen ions," *J. Quant. Spectrosc. Radiat. Transf.*, vol. 149, pp. 360–371, 2014.
- [9] Priti *et al.*, "Calculation of fully relativistic cross sections for electron excitation of cesium atom and its application to the diagnostics of hydrogen-caesium plasma," *J. Quant. Spectrosc. Radiat. Transf.*, vol. 187, pp. 426–442, 2017.
- [10] A. K. Belyaev *et al.*, "Theoretical study of electronic excitation, ion-pair formation, and mutual neutralization in cesium-hydrogen collisions," *Phys. Rev. A*, vol. 90, p. 062701, Dec 2014.
- [11] M. Bacal *et al.*, "The negative ion mean free path and its possible implications," *AIP Conference Proceedings*, vol. 1390, pp. 13–21, 2011.
- [12] M. Barbisan *et al.*, "Laser absorption spectroscopy studies to characterize cs oven performances for the negative ion source SPIDER," *Journal of Instrumentation*, vol. 14, pp. C12011–C12011, dec 2019.
- [13] M. Barbisan *et al.*, "Development and first operation of a cavity ring down spectroscopy diagnostic in the negative ion source spider," *Review of Scientific Instruments*, vol. 92, p. 053507, 2021.
- [14] M. Spolaore *et al.*, "Design of a system of electrostatic probes for the RF negative ion source of the SPIDER experiment," *Journal of Physics D: Applied Physics*, vol. 43, p. 124018, mar 2010.
- [15] G. Serianni *et al.*, "Spatially-resolved diagnostics for optimisation of large ion beam sources," *Submitted to Review of Scientific Instruments*.